frontiers | Frontiers in Earth Science

ORIGINAL RESEARCH
published: 16 May 2022
doi: 10.3389/feart.2022.922664

Geometry and Kinematics Characteristics of Strike-Slip Fault Zone in Complex Structure Area: A Case Study From the South No. 15 Strike-Slip Fault Zone in the Eastern Sichuan Basin, China

Xiaoyun Cheng[1,2,3], *Wenlong Ding*[1,2,3]*, *Lei Pan*[4], *Yutao Zou*[4], *Yuntao Li*[1,2,3], *Yixing Yin*[1,2,3] *and Shihao Ding*[1,2,3]

[1]School of Energy Resources, China University of Geosciences, Beijing, China, [2]Beijing Key Laboratory of Unconventional Natural Gas Geological Evaluation and Development, China University of Geosciences, Beijing, China, [3]Key Laboratory of Strategy Evaluation for Shale Gas, Ministry of Natural Resources of the People's Republic of China, China University of Geosciences, Beijing, China, [4]Sinopec Exploration Company, Chengdu, China

OPEN ACCESS

Edited by:
Lei Gong,
Northeast Petroleum University, China

Reviewed by:
Jingshou Liu,
China University of Geosciences Wuhan, China
Jianhua He,
Chengdu University of Technology, China

***Correspondence:**
Wenlong Ding
dingwenlong2006@126.com

Specialty section:
This article was submitted to Economic Geology, a section of the journal Frontiers in Earth Science

Received: 18 April 2022
Accepted: 25 April 2022
Published: 16 May 2022

Citation:
Cheng X, Ding W, Pan L, Zou Y, Li Y, Yin Y and Ding S (2022) Geometry and Kinematics Characteristics of Strike-Slip Fault Zone in Complex Structure Area: A Case Study From the South No. 15 Strike-Slip Fault Zone in the Eastern Sichuan Basin, China. Front. Earth Sci. 10:922664. doi: 10.3389/feart.2022.922664

The eastern Sichuan Basin has undergone multiple stages of tectonic evolution and shows complex structural characteristics. It is found that there are a series of NW-SE base-trending strike-slip faults in this area besides NE-SW strike-blocking structures. There are almost no previous studies on strike-slip faults in the eastern Sichuan Basin. This paper fills in the blank of geometry and kinematics research on the strike-slip fault zone in this area. Based on highly precise 3D seismic section, coherent attribute slice and time slice, the geometric and kinematic characteristics of the fault are analyzed. The dynamic characteristics are analysed based on the structural style of the superimposed development model and the nature and activity intensity of strike-slip faults in different periods. and it was found that No. 15 strike-slip fault was a large basement strike-slip fault. The research results show that the profile of the No. 15 strike-slip fault mainly shows a subvertical fracture, positive flower structure and negative flower structure and a composite flower structure with positive and negative flower structures superimposed on each other in the upper and lower planar sections with linearly outspread and zonal distribution characteristics; spatially, there is a "ribbon" effect and a "dolphin" effect. the left strike-slip distance of the TS interface is 0.462 km, and the right strike-slip distance of the TP2 interface is 0.782 km. The strike-slip fault experienced at least three active stages of superimposed deformation during its formation and reconstruction, among which episode II in the middle Caledonian movement was the main active stage of the No. 15 strike-slip fault zone. This study of the structural style and genetic mechanism of a strike-slip fault zone is of guiding significance to the exploration and development of strike-slip fault-controlled reservoirs in the study area.

Keywords: geometry, kinematics, seismic attribute, sichuan basin, strike-slip fault

INTRODUCTION

The characteristics and structural styles of strike-slip faults have been characterized carefully in many literatures (Tchalenko, 1970; Sylvester, 1988; Mcclay and Bonora, 2001; Mitra and Paul, 2011; Dooley and Schreurs, 2012; Moscariello et al., 2017). In the recent years, more and more attention has been paid to the geometry and kinematics characteristics of strike-slip fault zone and a series of oil and gas exploration achievements related to strike-slip faults (Fisher and Knipe, 2001; Laubach et al., 2019; Torabi et al., 2019). A variety of different construction styles can occur simultaneously on one strike-slip fault zone, and these structural styles can be interpreted as the segmented nature of a strike-slip fault (Peacock, 1991; Dooley and Schreurs, 2012; Jiao, 2017; Qi, 2020; Zeng et al., 2022), however, the factors controlling segmentation are rarely discussed, especially for strike-slip faults developed in complex structural areas. On strike-slip fault zones in complex structural areas, due to the tectonic movement of different mechanical properties, the formation lithology is different, the faults usually show the characteristics of regional detachment strata-bound. Strike-slip faults formed in the early stage can be activated and subsequently developed upwards in the later stage, and the development characteristics of structural styles formed in the early stage will also affect the late structural deformation.

The eastern Sichuan Basin is characterized by a series of nearly parallel, highly steep anticlinal fold belts, with multiple sets of regional detachment layers and multiple deep and large basement faults in the region (Wang et al., 2015; Pan et al., 2020). Since the Proterozoic, the study area has experienced multiple periods of tectonic movement, and these periods can be divided into several structural layers bounded by detachment layers and various developed structural styles. In the early stage of oil and gas exploration in the Sichuan Basin, major breakthroughs were made with Permian and Triassic as the main exploration targets. In recent decades, domestic oil and gas exploration research has gradually shifted in an unconventional direction, and the exploration and development prospects of black shale reservoirs in the Lower Silurian Longmaxi Formation of the Sichuan Basin are very broad (Tong et al., 2015; Wang et al., 2016; Tuo et al., 2020). Shale fractures can serve as effective storage spaces and rapid migration channels for natural gas and the formation of water. In marine organic-rich brittle shale of lower Palaeozoic age in the Sichuan Basin, wells displaying good natural gas production are closely related to fracture development (Fisher and Knipe, 2001; Ding et al., 2012; Cao and Neubauer, 2016; Deng et al., 2019).

As the strike-slip fault-controlled reservoirs in the Tarim Basin have facilitated major oil and gas exploration breakthroughs (Han et al., 2017; Jiao, 2017; Deng et al., 2018; Wang et al., 2019), the control and transformation of strike-slip faults in the Sichuan Basin should be highly valued (Ding et al., 2020).The purposes of this study are to 1) describe the structural geometry characteristics of the southern segment of the No. 15 strike-slip fault zone, 2) discuss the strike-slip directions and distances of this fault zone through kinematic analyses, and 3) understand the active periods and tectonic evolution characteristics of the analysed strike-slip fault zone.

GEOLOGIC SETTING

The Sichuan Basin, located in southwestern China (**Figure 2C**), is a superimposed basin developed on the foundation of the upper Yangtze craton, with a total area of approximately 260,000 km^2. This basin displays a rhomboid-shaped geometry in map view and is bounded by the Qiyueshan fault zone to the southeast, the Longmenshan thrust belt to the northwest, Micang Mountain and Daba Mountain to the northeast, and the Kangdian thrust fold belt to the southwest (**Figure 2A**). Based on basement structure, primary basement faults, and sediment distribution, the Sichuan Basin can be divided into 6 tectonic units, including depressions, uplifts and fold belts. From north to south, these units are the Chuannan fold structural belt, Chuandong highly steep folded structural belt, Chuandongbei Composite highly steep folded structural belt, Chuanzhong uplift, Chuanxi depression, and Chuanxinan fold structural belt.

The Sichuan Basin has undergone multistage tectonic evolution, and the study area has experienced extensive compression, extension and shear deformation processes (Li and Li, 2007; Wang et al., 2007; Chu et al., 2012; Zheng et al., 2020). The Jiangnan-Xuefeng uplift orogenic belt was formed during the middle Caledonian movement (Middle Ordovician to Late Ordovician) on the south-eastern margin of eastern Sichuan. During the late Caledonian movement, NW-SE compressive stress occurred due to the NW subduction of the Pacific plate, and NE-SW compressive stress was also formed due to the NW subduction of the Yunnan-Tibetan Oceanic plate (Chu et al., 2012; Hong et al., 2020). After the Caledonian movement, because the northern North Qinling Ocean gradually closed from east to west, sea water gradually exited the Upper Yangtze region. Throughout the early Hercynian movement (during the lower Permian in the Palaeozoic sedimentary period), the eastern Sichuan region inherited the structural relief of the Caledonian movement period (Yin et al., 2018; Li et al., 2020; Chen et al., 2021). At this time, the compressional stress was NS trending, and Devonian and Carboniferous strata were absent, resulting in disconformable contacts between the lower Permian strata and the Silurian strata (Wang et al., 2013; He et al., 2020). In the early stage of Indosinian movement (middle Triassic to Late Triassic), the Qinling orogenic belt and Jiangnan-Xuefeng tectonic belt were uplifted again, and sea water withdrew from eastern Sichuan to the northwest, completing the transition from marine Evaluation of sweet spots and horizontal-well-design technology for shale gas in the basin-margin transition zo Authigenic clay minerals and calcite dissolution influence reservoir quality in tight sandston to continental deposition environments (Zhao et al., 2021). The late Himalayan period was the final surface structural morphology period in the study area. At this time, the Dabashan thrust belt in the north-eastern margin of the study area formed an intense detachment-thrust structure (Xiao et al., 2011; Li et al., 2013; Yin et al., 2020; Liu J et al., 2022).

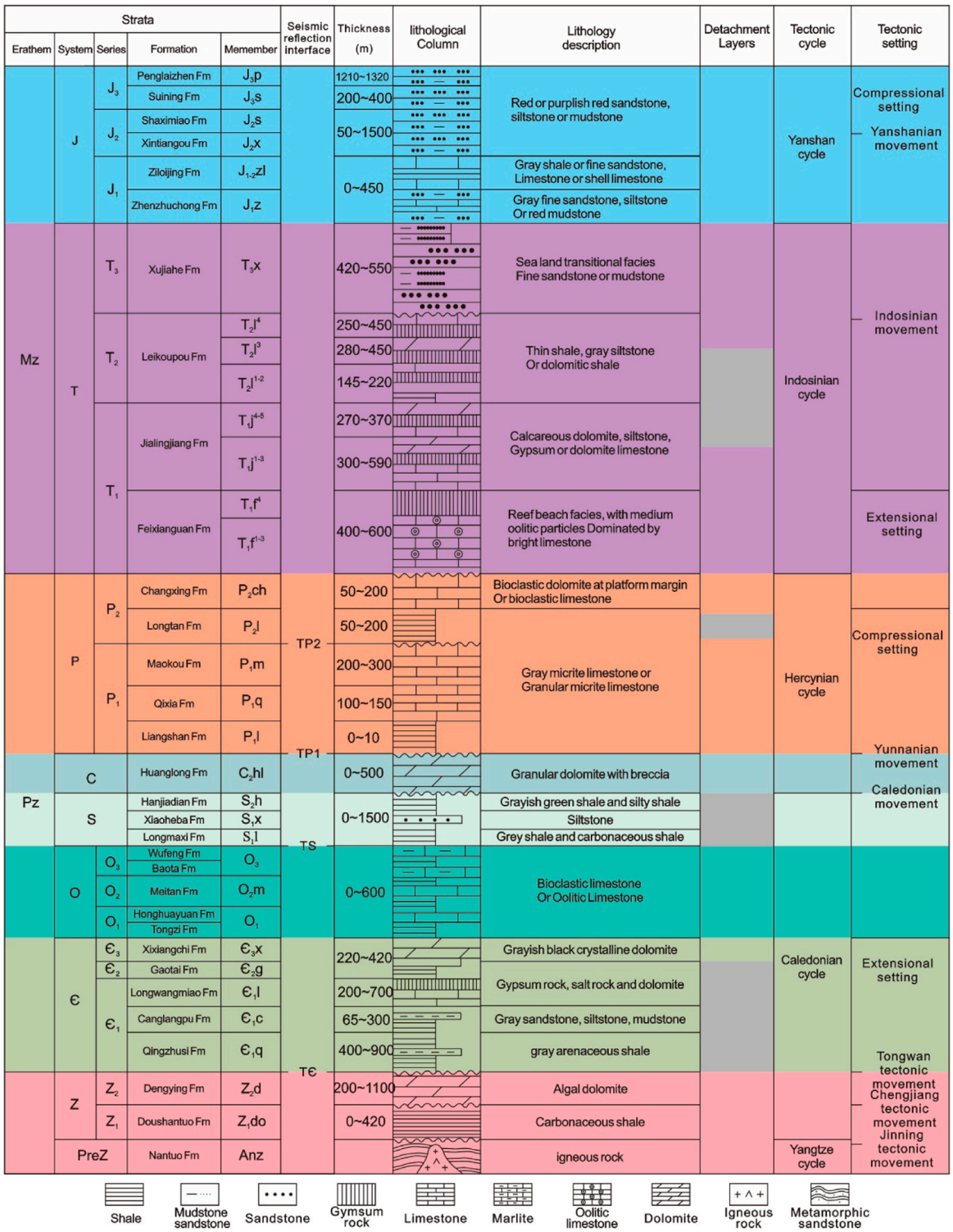

FIGURE 1 | Generalized stratigraphy, seismic reflecting surfaces, and tectonic movements of the Sichuan Basin (revised after Li et al., 2020).

The sedimentary strata in the Sichuan Basin are composed of two sequences, including Palaeozoic and Mesozoic sequences (**Figure 1**). The Sinian to Middle Triassic strata comprise marine carbonate deposits, while the Upper Triassic and shallow strata contain continental clastic deposits. At the end of the Sinian period, mangrove bay movement formed the

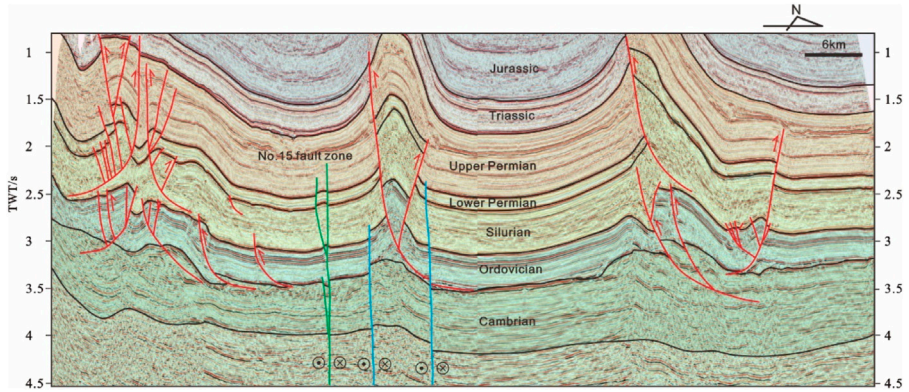

FIGURE 2 | Geological section map of Fuling work area in Sichuan Basin.

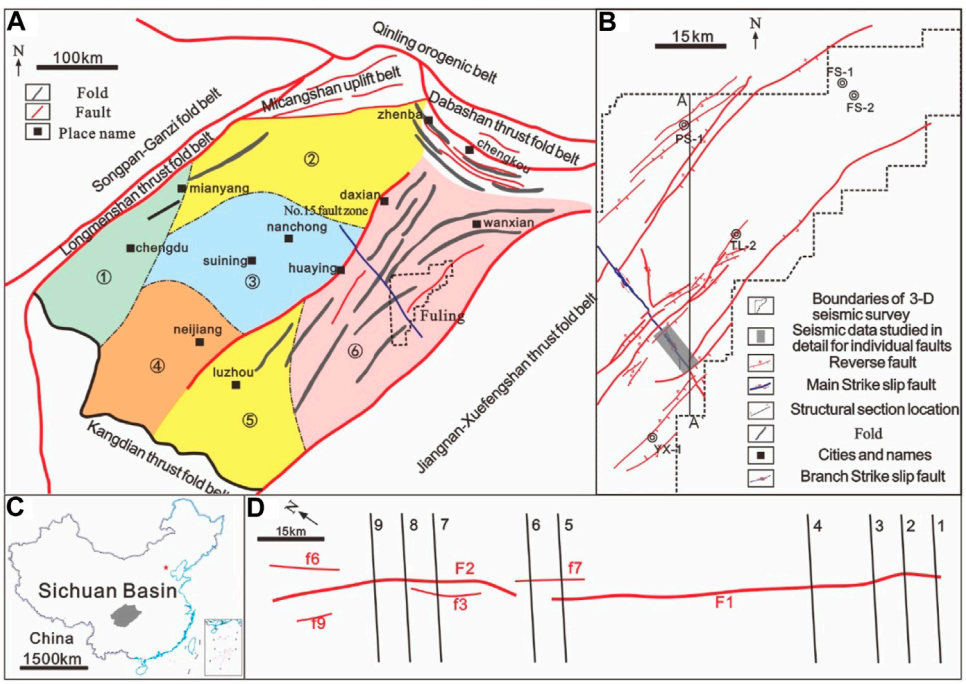

FIGURE 3 | (A) Simplified tectonic map showing the major tectonic units and fault distributions in Sichuan Basin, this basin covers an area of 26 × 10^4 km^2, ①: Chuanxi depression ②: Chuanbei Composite highly steep folded structural belt, ③: Chuanzhong uplift, ④: Chuanxinan fold structural belt ⑤: Chuannan fold structural belt, ⑥: Chuandong highly steep folded structural belt. **(B)** Fault distribution map of Fuling work area. **(C)** The location of the Sichuan Basin on a map of China. **(D)** Fault distribution map of the South No. 15 Strike-slip Fault Zone.

unconformity between the Cambrian and Sinian strata (Є—Z), and the upper Silurian, Devonian and Carboniferous strata were missing in the study area of the late Caledonian Movement, resulting in a pseudoconformity contact (O–P) between the Permian and lower Carboniferous strata. The unconformity between the Late Triassic and Middle Triassic and older strata represents the early stage of the Indosinian movement at the end of the Middle Triassic.

Three sets of stably distributed regional detachment layers are developed in the study area (Faure et al., 2008; Yin and Wu, 2020; Li et al., 2021), and the existence of a plastic detachment layer plays an important role in controlling the deformation of the thrust belt. From bottom to top, these sets include the gypsum-bearing lower to middle Cambrian Longwangmiao and Gaotai Formations, the mud shale of the Lower Silurian Longmaxi Formation, and the gypsum-bearing lower to middle Triassic Leikoupo and Jialingjiang Formations (Dong et al., 2011; Li et al., 2021). The stability of the detachment layer and difference in its spatial distribution lead to the differential stratification-deformation characteristics in eastern Sichuan. The seismic data of the Lower Cambrian and the corresponding lower strata are of poor quality. According to the existing 3D seismic

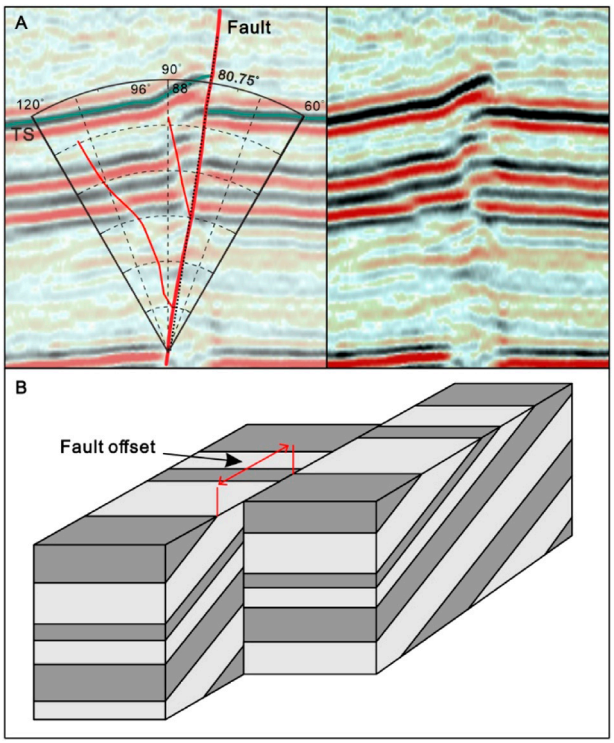

FIGURE 4 | (A) Explanation of the methodology used for the measurement of the Tendency change and **(B)** a schematic model showing that horizontal displacement of strike slip fault on the horizontal plane or time slice.

data, the deep strata in the study area are relatively gentle with a low deformation degree. Multirow NE-trending structures controlled by NE-trending main faults are developed, and NW-trending basement faults may be developed (Pan et al., 2020). Multiple sets of compression-detachment structures developed in the Central Triassic to Silurian, including Y-shaped faults, anti-Y-shaped faults, and back-thrust structures (Wu et al., 2019). The Silurian strata with strong plasticity have obvious secondary thickening at the top of the middle structural layer (Wang et al., 2018; Gong et al., 2019; Lan et al., 2021), thus exerting strong control over the formation of strike-slip fault flower structures (Yin et al., 2020; Liu J. et al., 2022). Because of the uneven spatial distribution of the detachment layer, there are two types of detachment in the study area: single-layer detachment and double-layer detachment (Yan et al., 2003; Li et al., 2012; Gong et al., 2021; Li, 2022; **Figure 3**). The Jurassic and shallow strata developed a series of NNE-NE-trending arc-shaped barrier structures (**Figure 2A**).

DATA AND METHODS

The high-quality 3-D seismic data used in this study representing an area of 4000 km^2, was derived through a rectangular survey and covers part of the South No. 15 strike-slip fault zone (**Figure 2B**). The lines and traces are north–south- and east–west-oriented, respectively, and both have a 25-m spacing. The stratigraphic horizons are marked by seismic reflecting surfaces determined by integrating well log and seismic data. The Tϵ, TS, TP1, and TP2 seismic surfaces mark the bottom boundaries of the Cambrian, Silurian, Lower Permian and Upper Permian strata, respectively. The No. 15 strike-slip fault zone was recognized and interpreted in the local 3-D seismic sections perpendicular to the fault zone strike. The interpreted area is approximately 77 km^2. The interpretation spacing is 436 m. Using 3D seismic data to extract coherent attributes and time slices, the strike and development characteristics of the No. 15 strike-slip fault zone are described. Additionally, the dip angle of the master strike-slip fault is determined (**Figure 4A**). TS and TP2 horizon burial depth maps are prepared to characterize the stereo development along the strike of the No. 15 fault zone.

STRUCTURAL GEOMETIY OF THE SOUTH NO. 15 FAULT

The No. 15 fault zone is located in the eastern Sichuan Basin (**Figure 1A**) and has a straight trace in map view with a length of approximately 2.28 km. The azimuth is approximately 321°. Based on the interpretation of 3-D seismic data as well as coherence attribute slice and time slice analyses, the plane, section and spatial geometric characteristics of the south No. 15 strike-slip fault zone are investigated in detail and presented as follows.

Geometry of the South No. 15 Strike-Slip Fault Zone in Plane View

In the study area, the No. 15 fault zone displays different patterns at various depths (**Figure 5**). On the TS seismic surface, the No. 15 fault zone is characterized by two main faults and four branch faults (**Figure 5A**). To the north of the F2 fault, the faults are NW-trending, with orientations ranging from 320° to 325°; the branch fractures F6 and F9 and the main fracture F2 are arranged parallel or subparallel to each other; and to the south, the F2 fault bends clockwise, with the fault trending NNW. The F1 fault is approximately straight, and the faults are stable and NW-trending, with orientations of 321° and undeveloped branch faults. On the TP2 seismic surface, the No. 15 fault zone is composed of two main faults and three branch faults (**Figure 5B**). The strike of the fault is variable and roughly NW-trending. Similar to the feature shown on the TS surface, to the north of the F2 fault, the faults are NW-trending, and to the south, the F2 fault bends clockwise, with the fault trending approximately NNW at an orientation of 332°.

The horizontal time slice shows that the strike-slip fault offsets the TS surface and TP2 surface (**Figures 5,6**). On the 2500-ms time slice, the TS surface implies a left-lateral slip sense (**Figure 5C**). On the 3220-ms time slice, the TP2 surface implies a right-lateral slip sense, and the TS surface in the lower right corner still suggests a left-lateral slip sense (**Figure 5D**).

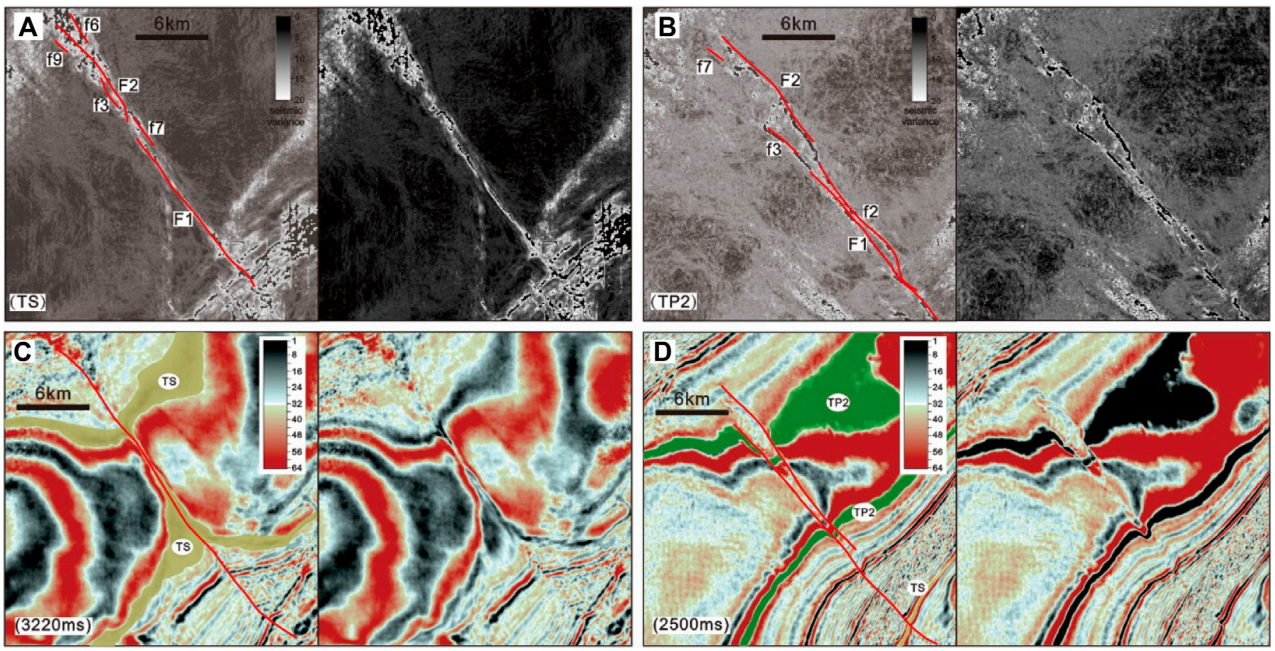

FIGURE 5 | Interpreted (left) and uninterpreted (right) variance slices of the **(A)** TS seismic surfaces, **(B)** TP1 seismic surfaces, **(C)** 3220 ms horizontal time slice and **(D)** 2500 ms horizontal time slice covering the south No. 15 fault zone. See the shadow box in **Figure 1B** for location.

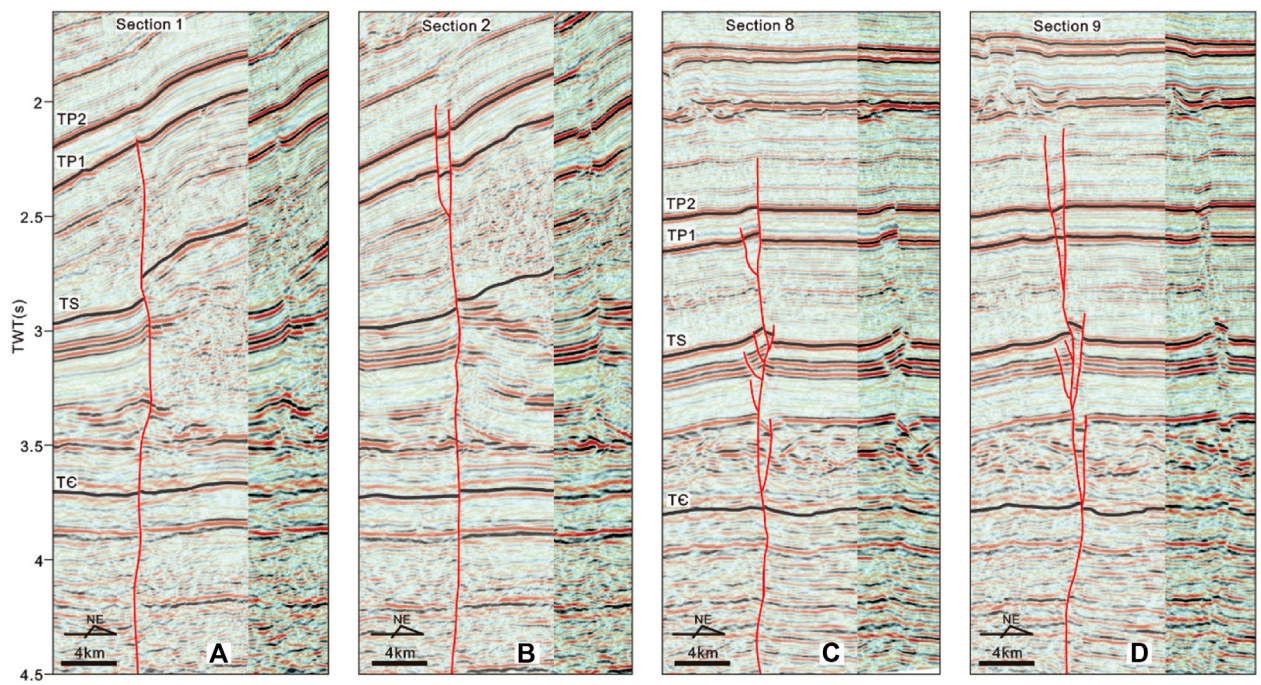

FIGURE 6 | Fault interpretations of cross Section 1**(A)**, Section 2**(B)**, Section 8**(C)**, Section 9**(D)**. The uninterpreted right images are shown for comparison and cropped as the central part of the left images where fault zones occur. See **Figure 1D** for location. TWT = two-way time.

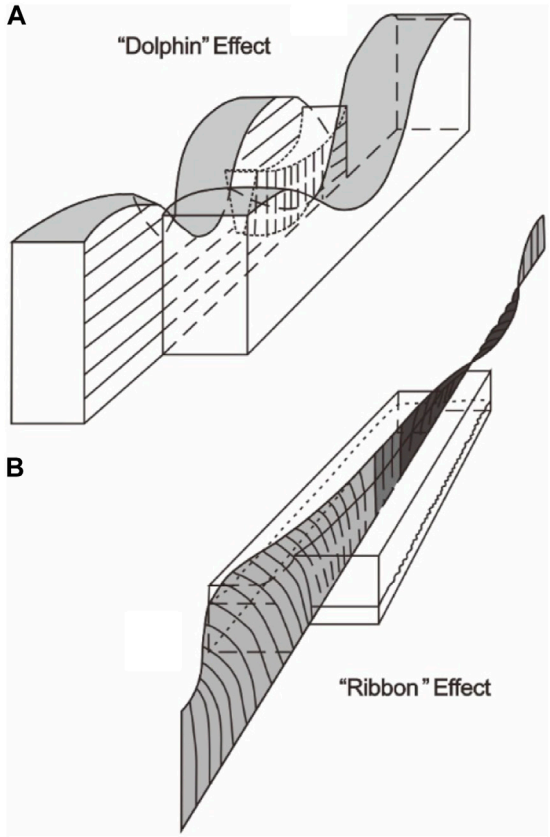

FIGURE 7 | Patterns of dolphin effect **(A)** and Ribbon effect **(B)**.

Structural Styles of the South No. 15 Strike-Slip Fault Zone in Seismic Sections

In section view, the main fault of the No. 15 fault zone appears to be subvertical (**Figures 6**,**8**). Upward, it diverges and extends through the TP2 seismic surface, and downward, it cuts through the Tϵ and terminates on the Presinian crystalline basement. The structural styles vary significantly vertically; the structural styles in the strata in the vicinity of the TP2 surface, TS surface and Tϵ surface are characterized in detail below.

Along the strike of No. 15, the structural styles in the strata in the vicinity of the TP2 seismic surface can be classified into two main types based on the corresponding structural relief (**Figure 6**): positive relief and negative relief. In the areas of positive relief, the strata were uplifted, and the majority of the uplifted strata were bounded by two or more small-scale faults with obvious reverse separation (**Figure 6C**). These small-scale faults developed downward onto the main fault to form a positive flower structure. These small-scale faults developed near TP2 merged downward onto the main subvertical fault to form a normal flower structure. On the seismic section, this structure is shown as a fracture zone with a gentle and wide upper section and a steep and narrow lower section oriented straight into the basement in the shape of a flower.

In the areas of negative relief, the strata were extended and subsided, and the subsidence area was bounded by two small-scale faults with normal separation (**Figure 6B**). Downward, they merge at depth into the main subvertical fault, usually terminating near the TS-to-TP1 package, defining a negative flower structure. Notably, in some seismic sections (e.g., **section 1**, **Figure 6A**), the main subvertical fault terminates near the TP1 surface, and on opposite sides of the subvertical fault, the strata are nearly horizontal.

Near the TS surface, the strata were uplifted, and the majority of the uplifted strata were bounded by some small-scale faults with obvious reverse separation. Downward, they merge at depth into the main subvertical fault commonly cutting through the Tϵ to TS package to define a positive flower structure. Additionally, in some seismic sections (e.g., **Sections 1**,**2**, **Figures 6A**,**B**), no positive flower structure is developed near the TS surface due to the vicinity to the thrust structural belt, and the vertical separation of strata on both sides of the fault is large.

Below the Tϵ surface, the strata in the vicinity of the main subvertical fault were shortened and uplifted. In addition, a positive flower structure and negative flower structure can be vertically superimposed in the same strike-slip fault zone. The positive flower structure developed near the deep TS surface, and the negative flower structure developed near the shallow TP2 surface, constituting a composite flower structure.

According to the vertical structural style differences found in the No. 15 fault zone described above, the strata in the study area can be divided into three strata combinations: 1) the lower combination consisting of the strata below the Tϵ surface, 2) the middle combination including the Tϵ-to-TS package, and 3) the upper combination composed of the TS-to-TP2 package.

Distribution Characteristics of the South No. 15 Strike-Slip Fault Zone in Three-Dimensional Space

Strike-slip faults often have "ribbon" and "dolphin" effects in space. The "ribbon" effect refers to the condition in which strike-slip faults are nearly upright when observed on a large scale but their tendency changes along the strike direction, swinging from side to side like ribbons (**Figure 7A**). At the TS interface, the southern main fault tendency of the No. 15 strike-slip fault zone is NE-trending (**Figure 8a~ 8D**), and the northern main fault tendency changes to become SW-trending (**Figure 8e~ 8G**). The northernmost part of the strike-slip fault changes to a NE trend (**Figure 8H**). The dolphin effect refers to the phenomenon in which the properties of normal and reverse faults change when observed on different seismic sections perpendicular to the fault zone strike under the condition that strike-slip faults have the same dip; that is, the relative elevations and faults of adjacent seismic profiles change (**Figure 7B**). On the TP1 surface, in the south, the relative heights of the structures on both sides of the southern main fault are high in the west and low in the east (**Figure 8a~ 8C**). Along the strike of the fault in the north, the variation is high in the east and low in the

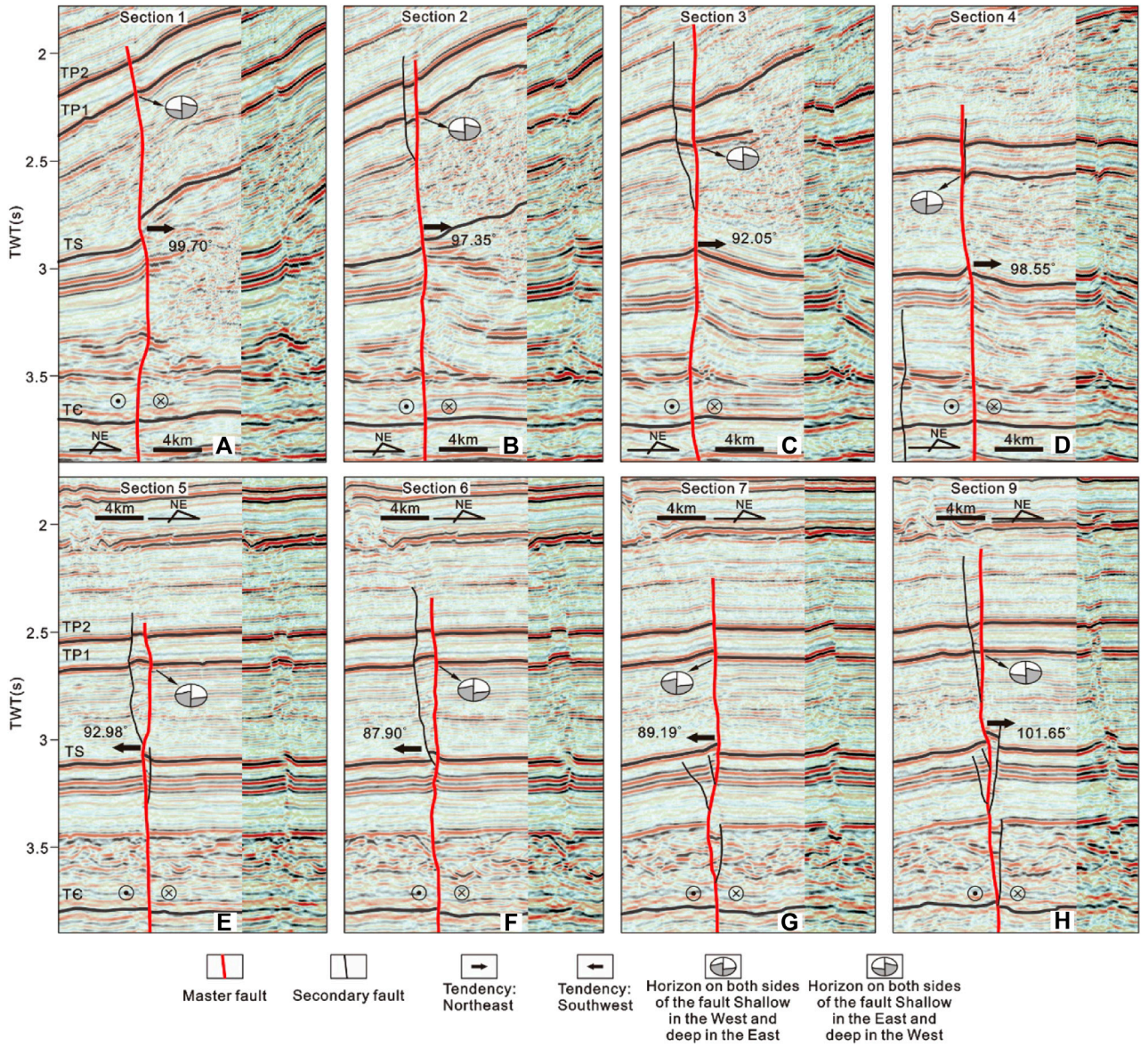

FIGURE 8 | Fault interpretations of cross Section 1**(A)**, Section 2**(B)**, Section 3**(C)**, Section 4**(D)**, Section 5**(E)**, Section 6**(F)**, Section 7**(G)**, Section 9**(H)**. The uninterpreted right images are shown for comparison and cropped as the central part of the left images where fault zones occur. See **Figure 1D** for location. TWT = two-way time.

west (**Figure 8d~8G**). The northernmost part of the interpretation boundary changes to reveal higher variations in the west and lower variations in the east (**Figure 8H**).

Through the statistics of the dip angles of F1 and F2, characterizing the two main faults in the South No. 15 strike slip fault zone, line charts of the four main horizons of the two main faults tendencies were obtained, and the trends of these main faults change along the strike trend; mainly, in the south-west direction at the 6–7 and 17–18 sections, the trend of the main fault changes to NE (**Figure 9**). The frequency distribution of the dip angles of the main faults shows that the dip angles are concentrated between 88° and 96°.

According to an analysis of temporal structural maps of the TS surface and TP2 surface, on the TP2 surface, the relative uplift relationship between the strike-slip faults and the strata on both sides is transformed. A long and wide anticline appears to the left of the main fault F2 (**Figure 10C**); southward, the stratum sandwiched between main fault F1 and branch fault f2 shows a long syncline (**Figure 10D**), indicating that the properties of normal and reverse faults have changed. On the TS surface, the relative uplift relationship of the stratum on both sides of the main strike-slip fault is reversed (**Figures 8E,F**). The northern anticline of the F2 main fault appears on the right side,

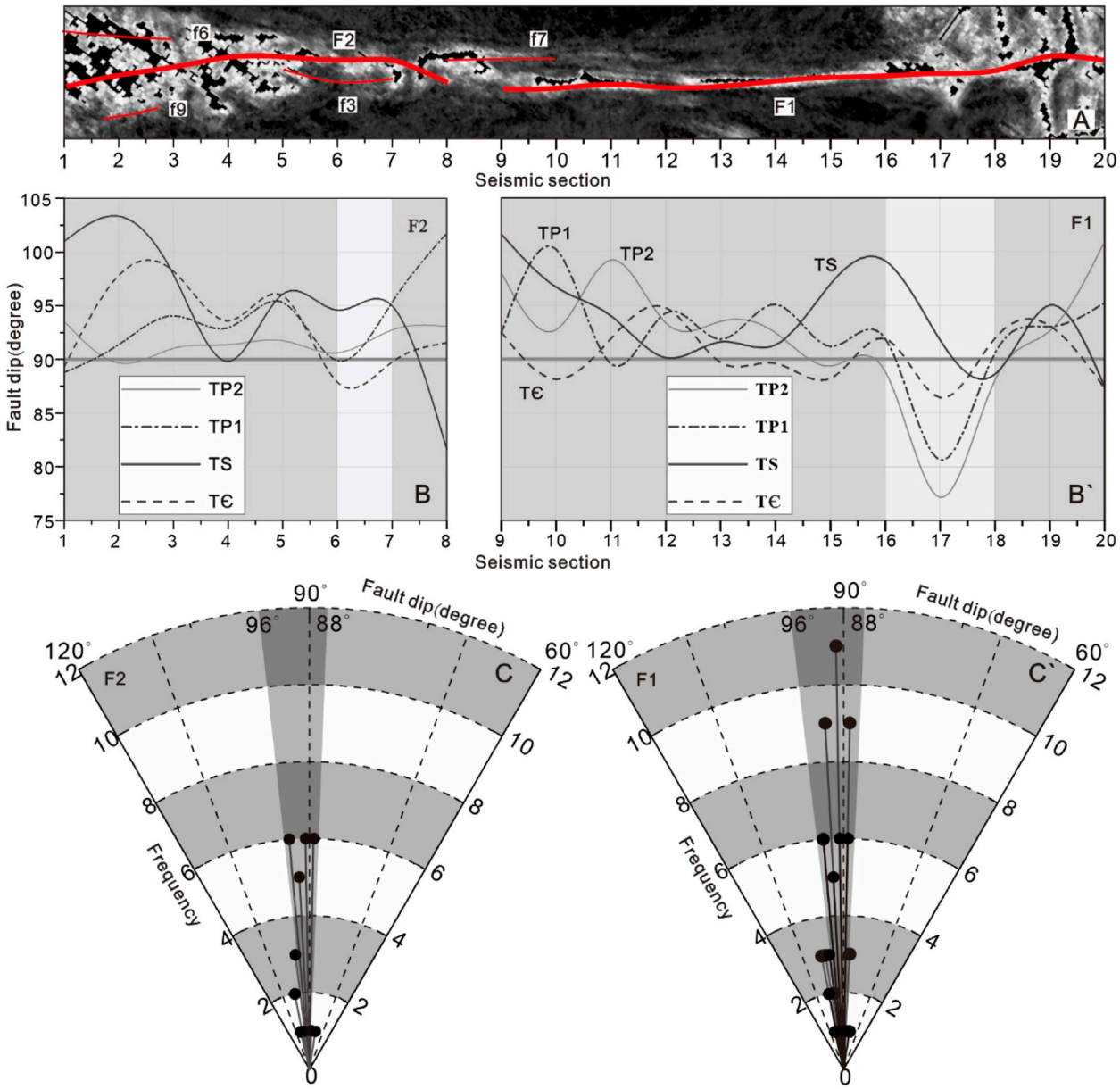

FIGURE 9 | (A) Plane distribution map of fault zone, Line chart of dip Angle variation of main fault F2 **(B)** and F1 **(B')** and Dip frequency distribution diagram of F2 **(C)** and F1 **(C')**.

and along the southward direction, an anticline with a small uplift appears on the left side (**Figure 10E**). These position changes in the anticlines on both sides of the F1 fault are similar to those shown in **Figure 10E**but are more obvious (**Figure 10F**). This result indicates that along the trend of the analysed strike-slip fault zone, the relative uplift relationship of strata on both sides of the fault changes. These phenomena indicate that the No. 15 strike-slip fault zone has a "dolphin" effect. For strike-slip faults without secondary faults, synclines are developed on both sides of the faults (**Figure 10G**).

STRUCTURAL KINEMATICS OF THE SOUTH NO. 15 FAULT

The kinematic characteristics of a strike-slip fault zone mainly include the strike-slip direction and the strike-slip distance. The horizontal dislocation of the geological boundary between the two plates of the analysed strike-slip fault zone was observed on a temporal slice to determine the strike-slip direction and the strike-slip distance of the strike-slip fault zone. In the horizontal time slice of 2500 ms (**Figure 11A**), it can be seen that on the TP2 interface, the wavelet signatures of the northeast

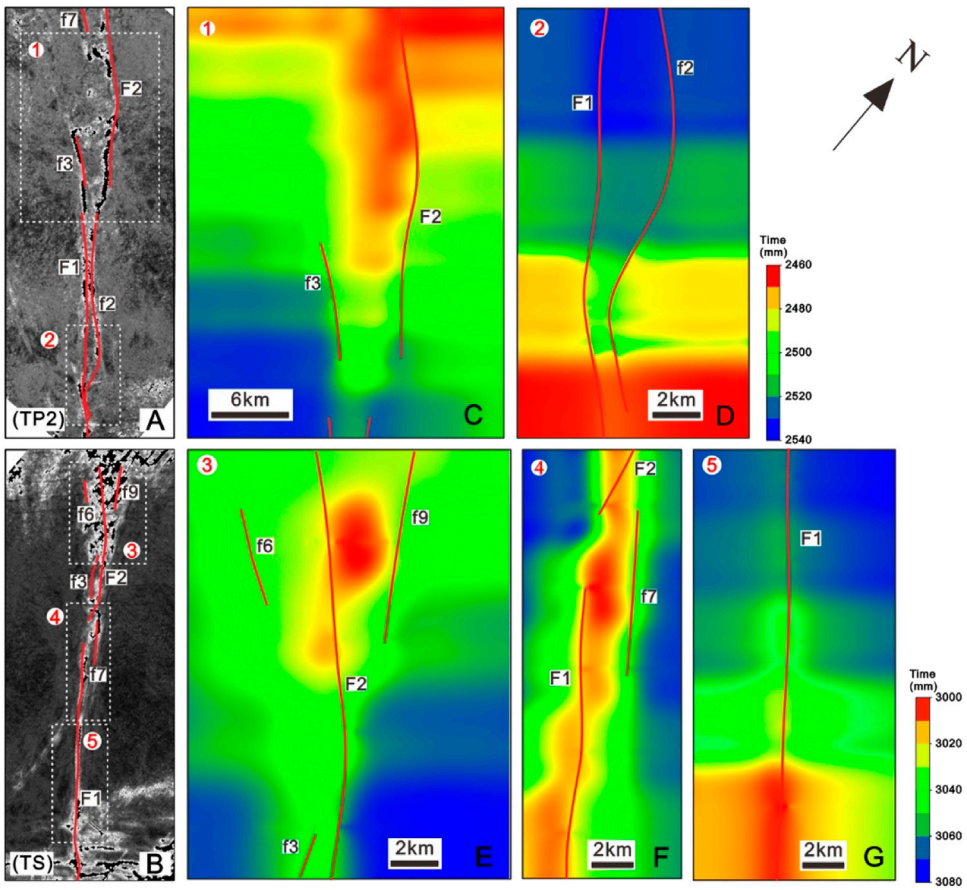

FIGURE 10 | Time structure maps (milliseconds) of the TP2 **(C,D)** and TS **(E–G)** seismic surfaces covering the south No.15 fault zone, showing the structural relief along the south No. 15 fault zone at various depths [see **(A)** and **(B)** for the locations of **(C–G)**], The depth data used in the map came from TS and TP2 interpretation data of 3D seismic data in the study area.

wall of the fault slid to the right relative to the wavelet signatures of the southwest wall. According to the offset of the wavelet signatures displayed on the horizontal time slice, the offset of fault No. 15 is measured to be 0.782 km (**Figure 11A**), characterizing a typical right-lateral strike-slip fault, and the stratum in the middle of the fault reflects negative relief. The TS surface at a depth of 3220 ms in the horizontal time slice (**Figure 11B**) was offset by a strike-slip fault, and the fault offset of fault No. 15 was measured to be 0.462 km (**Figure 11B'**), indicating left-lateral strike-slip properties. The results show that the No. 15 strike-slip fault zone was a left-lateral strike-slip fault when deposited in Silurian strata but a right-lateral strike-slip fault when deposited in Longtan Strata.

DISCUSSION

The active periods of strike-slip faults are analysed through the intersecting relationships between the strike-slip faults and active events. Since the active period of the analysed faults occurred later than the development period of the cut strata and earlier than that of the strata terminated by faults, the active times of the faults can be determined by determining the oldest cut strata and latest strata terminated by the strata (Wenzheng et al., 2012; Liu Y et al., 2022). The deepest part of the No. 15 strike-slip fault penetrates to the pre-Sinian crystalline basement, and the shallow part ends at the detachment layer of the Triassic Jialingjiang Formation (**Figure 12**). Therefore, the formation period of the No. 15 strike-slip fault zone was later than the formation period of the pre-Sinian crystalline basement, and the latest active period was earlier than the Early Triassic.

After multiple periods of tectonic evolution, a variety of vertically contraposed tectonic styles formed under different stress states in each multistage active period (**Figure 12**). By analysing the superimposed development mode of the vertical structural style of the strike-slip fault zone, the formation and evolution stages and the stress properties of different stages of the strike-slip fault zone can be qualitatively analysed. According to different tectonic styles and different stress field conditions, it can be concluded that the No. 15 strike-slip fault zone has experienced at least three active stages of superimposed deformation.

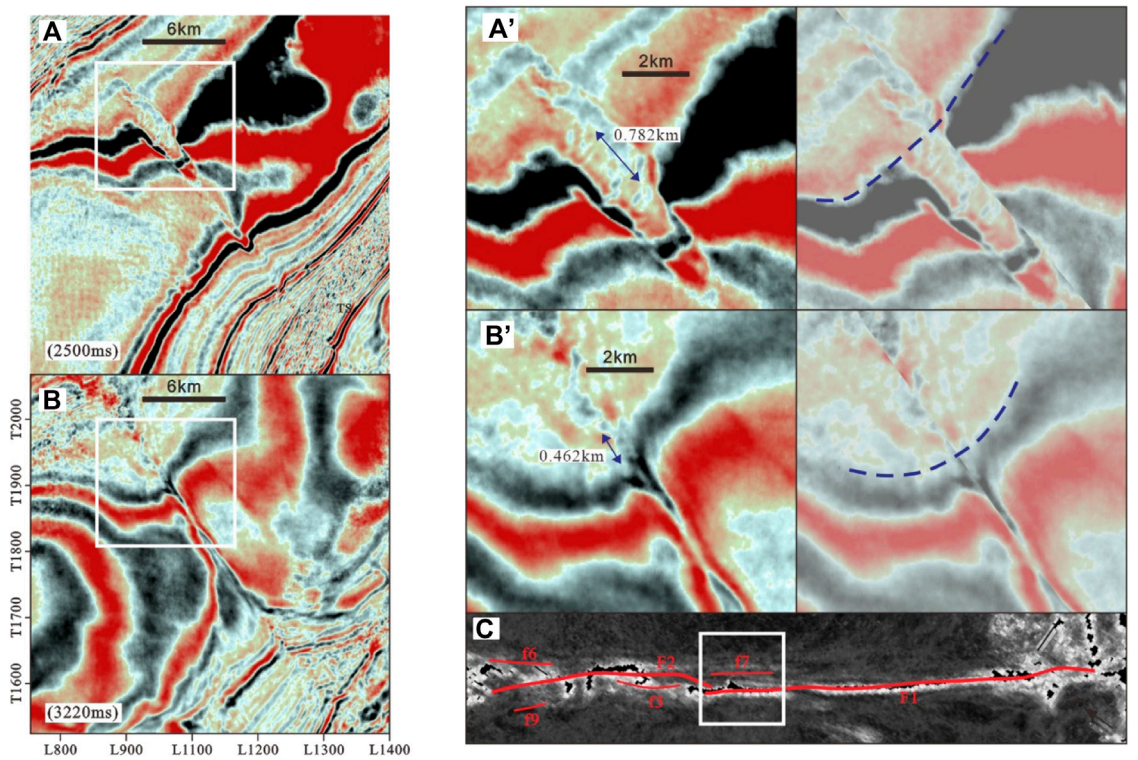

FIGURE 11 | (A) Horizontal time slice at 2500 ms and **(B)** Horizontal time slice at 3220 ms [see **(C)** for the locations of **(A)** and **(B)**]. **(A`)** Horizontal time slice at 2500 ms showing the discontinuous strata offset by the northern No. 15 fault and restoration of original continuous strata. **(B`)** Horizontal time slice at 3220 ms showing discontinuous strata offset by the southern SB5 fault and restoration of original continuous strata [see **(A)** and **(B)** for the locations of **(A`)** and **(B`)**].

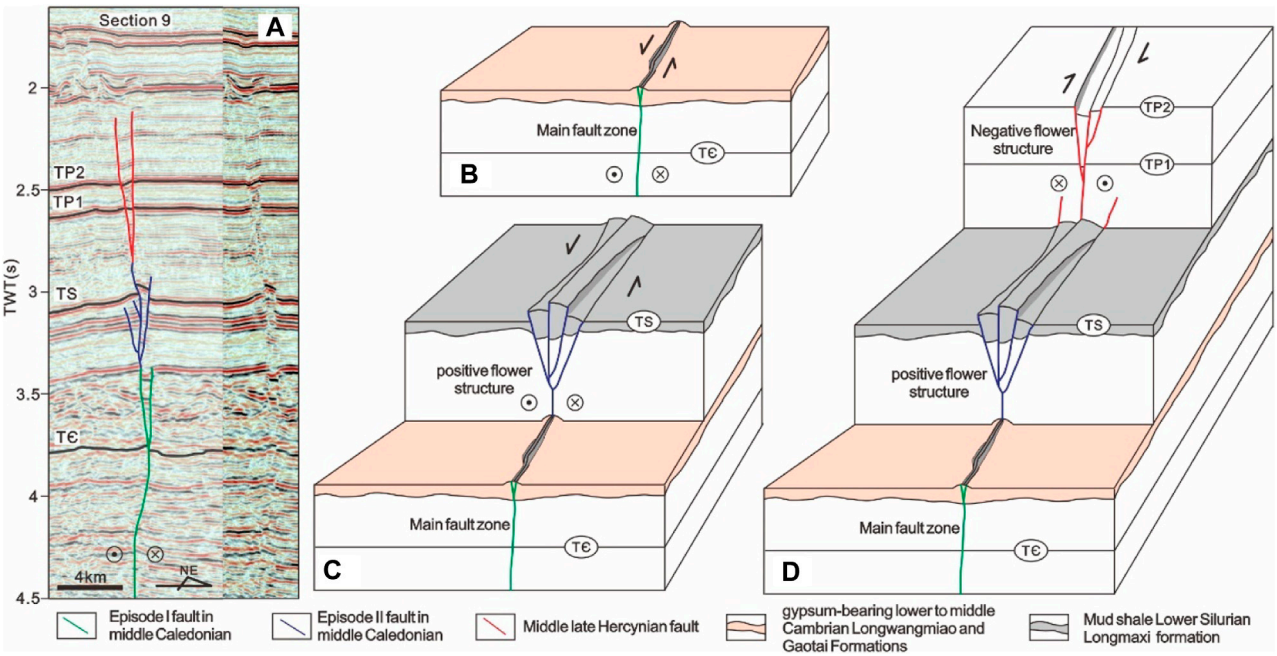

FIGURE 12 | (A) Fault interpretations of cross Section 9 (**Figure 3** for the definition of surfaces) and **(B)–(D)** Schematic model showing the structural evolution of individual strike-slip fault zones within a three-dimensional perspective.

The Middle Ordovician

During the Middle Ordovician, the Jiangnan-Xuefeng uplifted orogenic belt formed on the south-eastern margin of eastern Sichuan due to Act I of the Middle Caledonian Movement, and a strike-slip fault began to develop in the basement of the study area. A series of faults and anticlines developed above the Tϵ interface (**Figures 11B' 12B**). In these sections, strike-slip faults are characterized by near-vertical faults and the formation of flower structures (**Figures 6**,**8**,**12A**).

Notably, the deformation amplitude of the strata above the Tϵ interface is significantly greater than that below the Tϵ interface, and both positive and negative flower structures developed simultaneously. This phenomenon may be related to the presence of the gypsum-bearing lower-to middle-Cambrian Longwangmiao and Gaotai Formations.

The Late Ordovician

The strike-slip movement that occurred during the middle Act II of the Caledonian movement during late Ordovician deposition was the most intense. The pre-existing fault, a left-lateral strike-slip fault, on mid-Caledonian Act I continued to extend upward and develop inherently (**Figure 12C**), with the same strike direction as the deep fault. Multiple anticlines developed between multiple branch faults (**Figures 10E,F**), and the branch faults usually end at the upward TS interface; this characteristic is related to the existence of mud shale in the lower Silurian Longmaxi Formation (**Figure 3**).

The Lower Triassic

In the middle and late Hercynian study area during the Lower Triassic sedimentary period, the SN compression stress was the main action. The No. 15 strike-slip fault zone has undergone dextral strike-slip movement to reshape the pre-existing faults and is characterized by a series of faults and synclines near the TP2 interface. In these sections, strike-slip faults are characterized by flower-like structures (**Figures 6**,**8**,**12A**). The fault terminated upward at the plaster rock detachment layer of the gypsum-bearing lower to middle Triassic Leikoupo and Jialingjiang Formations, and then the strike-slip movement stopped.

The deep strata experienced multistage tectonic superimposed deformation. The striking difference between the strike-slip fault distance between the TS interface and TP2 interface is due to the different structural stages and strengths. The structural movement experienced by the same strike-slip fault in the later period can transform the strike-slip distance and reverse of the strike-slip fault formed in the early period due to its different strike-slip direction and strike-slip strength. as shown in **Figure 11**, the existing left-side strike-slip distance of the TS interface is 0.462 km (**Figure 11B**), and the existing right-side strike-slip distance of the TP2 interface is 0.782 km (**Figure 11A**). When describing the horizontal fault distance of the No. 15 strike-slip fault zone during the Late Ordovician deposition, the influence of right-lateral reconstruction should be eliminated. Because the No. 15 strike-slip fault zone terminated upward in the strata near the TP2 interface, the left-lateral strike-slip fault distance of the No. 15 strike-slip fault at the end of Act II of the Middle Caledonian Movement must eliminate only the influence of the right-lateral strike-slip movement that occurred in the middle to late Hercynian period; thus, the left-lateral strike-slip fault distance should be 1.244 km.

CONCLUSION

The South No. 15 fault zone has experienced multistage tectonic evolution and thereby displays complex structural styles. The controlling effect of the regional detachment layer causes the fault zone to be layered vertically, thereby displaying complex structural styles. In the cross-sectional view, the strike-slip faults are generally characterized by subvertical fault segments at depth (of Sinian to middle lower Cambrian age) and positive negative flower structures in the shallower strata (of Middle upper Ordovician to Permian age). Due to the existence of the detachment layer of the Jialingjiang Formation at the bottom of the overlying Triassic, the strike-slip fault did not continue to develop upward. In the later stage, the faults were inherited and developed, and the late structural deformation to the pre-existing structures, including the positive flower structures and negative flower structures, overlapped vertically. In map view, along-strike zones producing push-up or pull-apart structures can be commonly observed. In three-dimensional space, the dolphin effect and ribbon effect unique to strike-slip faults are also clearly displayed.

The South No. 15 fault zone experienced at least three strike-slip movements during the Palaeozoic. The first strike-slip movement occurred during the Middle Ordovician and was characterized by folding strata and the occurrence of subvertical fault segments. The second movement occurred during the period from the Late Ordovician. At this time, the strike-slip movement was the most intense, represented by the formation of a positive flower structure on the TS seismic surface. The third movement occurred during the period from the Late Silurian to Early Triassic and was characterized by the development of a negative flower structure cutting through the TP2 surface above the South No. 15 fault zone.

DATA AVAILABILITY STATEMENT

The original contributions presented in the study are included in the article/Supplementary Material, further inquiries can be directed to the corresponding author.

AUTHOR CONTRIBUTIONS

XC is responsible for the idea and writing of this paper and WD, LP, YZ, YL, YY, and SD are responsible for the data interpretation.

FUNDING

This research was supported by the National Natural Science Foundation of China (Grant Numbers 42072173) and the National Science and Technology Major Project of China (2016ZX05046-003–001).

ACKNOWLEDGMENTS

The authors would like to thank the staff of all of the laboratories that cooperated in performing the tests and analyses. We are also grateful to the reviewers, whose comments improved the quality of this manuscript.

REFERENCES

Cao, S., and Neubauer, F. (2016). Deep Crustal Expressions of Exhumed Strike-Slip Fault Systems: Shear Zone Initiation on Rheological Boundaries. *Earth-Science Rev.* 162, 155–176. doi:10.1016/j.earscirev.2016.09.010

Chen, G., Li, T., Yang, L., Zhang, G., Li, J., and Dong, H. (2021). Mechanical Properties and Failure Mechanism of Combined Bodies with Different Coal-Rock Ratios and Combinations [Mechanical Properties and Failure Mechanism of Combined Bodies with Different Coal-Rock Ratios and Combinations]. *J. Min. Strata Control Eng.* 3 (02), 84–94. doi:10.13532/j.jmsce.cn10-1638/td.20210108.001

Chu, Y., Faure, M., Lin, W., and Wang, Q. (2012). Early Mesozoic Tectonics of the South China Block: Insights from the Xuefengshan Intracontinental Orogen. *J. Asian Earth Sci.* 61, 199–220. doi:10.1016/j.jseaes.2012.09.029

Deng, S., Li, H., Han, J., Cui, D., and Zou, R. (2019). Characteristics of the Central Segment of Shunbei 5 Strike-Slip Fault Zone in Tarim Basin and its Geological Significance, [塔里木盆地顺北5号走滑断裂中段活动特征及其地质意义] [Article]. *Oil Gas Geol.* 40 (5), 990. Article 0253-9985(2019)40:5<990:Tlmpds>2.0.Tx;2-x. <Go to ISI>://CSCD:6590095. doi:10.11743/ogg20190504

Deng, S., Li, H., Zhang, Z., Wu, X., and Zhang, J. (2018). Characteristics of Differential Activities in Major Strike-Slip Fault Zones and Their Control on Hydrocarbon Enrichment in Shunbei Area and its surroundings,Tarim Basin, [塔里木盆地顺北及邻区主干走滑断裂带差异活动特征及其与油气富集的关系] [Article]. *Oil Gas Geol.* 39 (5), 878–888. Article 0253-9985(2018)39:5<878:Tlmpds>2.0.Tx;2-t. <Go to ISI>://CSCD:6358961. doi:10.11743/ogg20180503

Ding, W., Li, C., Li, C., Xu, C., Jiu, K., and Zeng, W. (2012). Dominant Factor of Fracture Development in Shale and its Relationship to Gas Accumulation, [页岩裂缝发育主控因素及其对含气性的影响] [Article]. *Earth Sci. Front.* 19 (2), 212–220. Article 1005-2321(2012)19:2<212:Ylffy>2.0.Tx;2-w. <Go to ISI>://CSCD:4520877.

Ding, Z., Wang, R., Chen, F., Yang, J., Zhu, Z., Yang, Z., et al. (2020). Origin, Hydrocarbon Accumulation and Oil-Gas Enrichment of Fault-Karst Carbonate Reservoirs: A Case Study of Ordovician Carbonate Reservoirs in South Tahe Area of Halahatang Oilfield, Tarim Basin. *Petroleum Explor. Dev.* 47 (2), 306–317. doi:10.1016/s1876-3804(20)60048-9

Dong, Y., Zhang, G., Neubauer, F., Liu, X., Genser, J., and Hauzenberger, C. (2011). Tectonic Evolution of the Qinling Orogen, China: Review and Synthesis. *J. Asian Earth Sci.* 41 (3), 213–237. doi:10.1016/j.jseaes.2011.03.002

Dooley, T. P., and Schreurs, G. (2012). Analogue Modelling of Intraplate Strike-Slip Tectonics: A Review and New Experimental Results. *Tectonophysics* 574-575, 1–71. doi:10.1016/j.tecto.2012.05.030

Faure, M., Lin, W., Monié, P., and Meffre, S. (2008). Palaeozoic Collision between the North and South China Blocks, Triassic Intracontinental Tectonics, and the Problem of the Ultrahigh-Pressure Metamorphism. *Comptes Rendus Geosci.* 340 (2-3), 139–150. doi:10.1016/j.crte.2007.10.007

Fisher, Q. J., and Knipe, R. J. (2001). The Permeability of Faults within Siliciclastic Petroleum Reservoirs of the North Sea and Norwegian Continental Shelf. *Mar. Petroleum Geol.* 18 (10), 1063–1081. doi:10.1016/s0264-8172(01)00042-3

Gong, L., Fu, X., Wang, Z., Gao, S., Jabbari, H., Yue, W., et al. (2019). A New Approach for Characterization and Prediction of Natural Fracture Occurrence in Tight Oil Sandstones with Intense Anisotropy. *Bulletin* 103 (6), 1383–1400. doi:10.1306/12131818054

Gong, L., Gao, S., Liu, B., Yang, J., Fu, X., Xiao, F., et al. (20212021). Quantitative Prediction of Natural Fractures in Shale Oil Reservoirs. *Geofluids* 2021, 1–15. Article 5571855. doi:10.1155/2021/5571855

Han, X., Deng, S., Tang, L., and Cao, Z. (2017). Geometry, Kinematics and Displacement Characteristics of Strike-Slip Faults in the Northern Slope of Tazhong Uplift in Tarim Basin: A Study Based on 3D Seismic Data. *Mar. Petroleum Geol.* 88, 410–427. doi:10.1016/j.marpetgeo.2017.08.033

He, X., Zhang, P., He, G., Gao, Y., Liu, M., Zhang, Y., et al. (2020). Evaluation of Sweet Spots and Horizontal-Well-Design Technology for Shale Gas in the Basin-Margin Transition Zone of Southeastern Chongqing, SW China. *Energy Geosci.* 1 (No.3-4), 134–146. doi:10.1016/j.engeos.2020.06.004

Hong, D., Cao, J., Wu, T., Dang, S., Hu, W., and Yao, S. (2020). Authigenic Clay Minerals and Calcite Dissolution Influence Reservoir Quality in Tight Sandstones: Insights from the Central Junggar Basin, NW China. *Energy Geosci.* 1 (No.1-2), 8–19. doi:10.1016/j.engeos.2020.03.001

Jiao, F. (2017). Significance of Oil and Gas Exploration in NE Strike-Slip Fault Belts in Shuntuoguole Area of Tarim Basin, [塔里木盆地顺托果勒地区北东向走滑断裂带的油气勘探意义] [Article]. *Oil Gas Geol.* 38 (5), 831–839. Article 0253-9985(2017)38:5<831:Tlmpds>2.0.Tx;2-f. <Go to ISI>://CSCD:6109642. doi:10.11743/ogg20170501

Lan, S., Song, D., Li, Z., and Liu, Y. (2021). Experimental Study on Acoustic Emission Characteristics of Fault Slip Process Based on Damage Factor [Experimental Study on Acoustic Emission Characteristics of Fault Slip Process Based on Damage Factor]. *J. Min. Strata Control Eng.* 3 (3), 82–90. doi:10.13532/j.jmsce.cn10-1638/td.20210510.002

Laubach, S. E., Lander, R. H., Criscenti, L. J., Anovitz, L. M., Urai, J. L., Pollyea, R. M., et al. (2019). The Role of Chemistry in Fracture Pattern Development and Opportunities to Advance Interpretations of Geological Materials. *Rev. Geophys.* 57 (3), 1065–1111. doi:10.1029/2019rg000671

Li, C., He, D., Lu, G., Wen, K., Simon, A., and Sun, Y. (2021). Multiple Thrust Detachments and Their Implications for Hydrocarbon Accumulation in the Northeastern Sichuan Basin, Southwestern China. *Bulletin* 105 (2), 357–390. doi:10.1306/07272019064

Li, H. (2022). Research Progress on Evaluation Methods and Factors Influencing Shale Brittleness: A Review. *Energy Rep.* 8, 4344–4358. doi:10.1016/j.egyr.2022.03.120

Li, J., Zhang, Y., Dong, S., and Shi, W. (2013). Structural and Geochronological Constraints on the Mesozoic Tectonic Evolution of the North Dabashan Zone, South Qinling, Central China. *J. Asian Earth Sci.* 64, 99–114. doi:10.1016/j.jseaes.2012.12.001

Li, S., Santosh, M., Zhao, G., Zhang, G., and Jin, C. (2012). Intracontinental Deformation in a Frontier of Super-convergence: A Perspective on the Tectonic Milieu of the South China Block. *J. Asian Earth Sci.* 49, 313–329. doi:10.1016/j.jseaes.2011.07.026

Li, Y., Zhou, D.-H., Wang, W.-H., Jiang, T.-X., and Xue, Z.-J. (2020). Development of Unconventional Gas and Technologies Adopted in China. *Energy Geosci.* 1 (No.1), 55–68. doi:10.1016/j.engeos.2020.04.004

Li, Z.-X., and Li, X.-H. (2007). Formation of the 1300-km-wide Intracontinental Orogen and Postorogenic Magmatic Province in Mesozoic South China: A Flat-Slab Subduction Model. *Geol* 35 (2), 179–182. doi:10.1130/g23193a.1

Liu, J., Yang, H., Xu, K., Wang, Z., Liu, X., Cui, L., et al. (2022). Genetic Mechanism of Transfer Zones in Rift Basins: Insights from Geomechanical Models. *GSA Bull.* doi:10.1130/b36151.1

Liu, Y., Chen, L., Tang, Y., Zhang, X., and Qiu, Z. (2022). Synthesis and Characterization of Nano-SiO2@octadecylbisimidazoline Quaternary Ammonium Salt Used as Acidizing Corrosion Inhibitor. *Rev. Adv. Mater. Sci.* 61 (1), 186–194. doi:10.1515/rams-2022-0006

Mcclay, K., and Bonora, M. (2001). Analog Models of Restraining Stepovers in Strike-Slip Fault Systems. *Aapg Bull.* 85 (2), 233–260. doi:10.1306/8626c7ad-173b-11d7-8645000102c1865d

Mitra, S., and Paul, D. (2011). Structural Geometry and Evolution of Releasing and Restraining Bends: Insights from Laser-Scanned Experimental Models. *Bulletin* 95 (7), 1147–1180. doi:10.1306/09271010060

Moscariello, A., Couto, D., Mondino, F., Booth, J., Lupi, M., and Mazzini, A. (2018). Genesis and Evolution of the Watukosek Fault System in the Lusi Area (East Java). *Mar. Petroleum Geol.* 90, 125–137. doi:10.1016/j.marpetgeo.2017.09.032

Pan, L., Xu, Z., Li, R., and Zou, Y. (2020). Basement Fault Characterization and Hydrocarbon Accumulation in Fuling of Southeastern Sichuan, [川东南涪陵地区基底断裂特征与油气成藏] [Article]. *Special Oil Gas Reservoirs* 27 (4), 19–25. Article 1006-6535(2020)27:4<19:Cdnfld>2.0.Tx;2-e. <Go to ISI>://CSCD:6835640.

Peacock, D. C. P. (1991). Displacements and Segment Linkage in Strike-Slip Fault Zones. *J. Struct. Geol.* 13 (9), 1025–1035. doi:10.1016/0191-8141(91)90054-m

Qi, L. (2020). Characteristics and Inspiration of Ultra-deep Fault-Karst Reservoir in the Shunbei Area of the Tarim Basin [Article]. *China Pet. Explor.* 25 (1), 102–111. doi:10.3969/j.issn.1672-7703.2020.01.010

Sylvester, A. G. (1988). Strike-slip Faults. *Geol. Soc. Am. Bull.* 100 (11), 1666–1703. doi:10.1130/0016-7606(1988)100<1666:ssf>2.3.co;2

Tchalenko, J. S. (1970). Similarities between Shear Zones of Different Magnitudes. *Geol. Soc. Am. Bull.* 81 (6), 1625–1640. doi:10.1130/0016-7606(1970)81[1625:sbszod]2.0.co;2

Tong, L., Ziquan, Y., Shugen, L., Zhiqiang, B., and Hao, W. (2015). Basic Characteristic of Shale of Wufeng-Longmaxi Formation in Shilin,southeast of Sichuan Basin. *J. Northeast Petroleum Univ.* 39 (3), 11.

Torabi, A., Alaei, B., and Libak, A. (2019). Normal Fault 3D Geometry and Displacement Revisited: Insights from Faults in the Norwegian Barents Sea. *Mar. Petroleum Geol.* 99, 135–155. doi:10.1016/j.marpetgeo.2018.09.032

Tuo, X., Chen, K., Luo, S., Tang, J., Zhang, D., and Shen, J. (2020). Structural Characteristics of Qiyueshan Fault and Shale Gas Preservation at the Southeastern Margin of Sichuan Basin, [四川盆地东南缘齐岳山断裂构造特征与页岩气保存条件] [Article]. *Oil Gas Geol.* 41 (5), 1017–1027. Article 0253-9985(2020)41:5<1017:Scpddn>2.0.Tx;2-1. <Go to ISI>://CSCD:6901823. doi:10.11743/ogg20200512

Wang, R., Ding, W., Zhang, Y., Wang, Z., Wang, X., He, J., et al. (2016). Analysis of Developmental Characteristics and Dominant Factors of Fractures in Lower Cambrian Marine Shale Reservoirs: A Case Study of Niutitang Formation in Cen'gong Block, Southern China. *J. Petroleum Sci. Eng.* 138, 31–49. doi:10.1016/j.petrol.2015.12.004

Wang, Z., Kang, N., Li, M., Zang, D., Zhang, Y., and Yang, X. (2018). Detached Structure Features in East Sichuan Basin. *Oil Geophys. Prospect.* 53(z1), 276–286. doi:10.13810/j.cnki.issn.1000-7210.2018.S1.044

Wang, R., Hu, Z., Long, S., Liu, G., Zhao, J., Dong, L., et al. (2019). Differential Characteristics of the Upper Ordovician-Lower Silurian Wufeng-Longmaxi Shale Reservoir and its Implications for Exploration and Development of Shale Gas In/around the Sichuan Basin. *Acta Geol. Sin. - Engl. Ed.* 93 (3), 520–535. doi:10.1111/1755-6724.13875

Wang, R., Leng, J., Ding, W., Gong, D., Li, F., and Sun, Y. (2015). Logging Identification of the Lower Cambrian Niutitang Shale Gas Reservoir in Upper Yangtze Region: A Case Study of the Cengong Block,Guizhou Province, [上扬子地区下寒武统牛蹄塘组优质页岩储层测井识别以贵州岑巩页岩气区块为例]. *Nat. Gas. Geosci.* 26 (12), 2395–2407. Article 1672-1926(2015)26:12<2395:Syzdqx>2.0.Tx;2-m. <Go to ISI>://CSCD:5619668. doi:10.11764/j.issn.1672-1926.2015.12.2395

Wang, Y., Fan, W., Zhang, G., and Zhang, Y. (2013). Phanerozoic Tectonics of the South China Block: Key Observations and Controversies. *Gondwana Res.* 23 (4), 1273–1305. doi:10.1016/j.gr.2012.02.019

Wang, Y., Fan, W., Zhao, G., Ji, S., and Peng, T. (2007). Zircon U-Pb Geochronology of Gneissic Rocks in the Yunkai Massif and its Implications on the Caledonian Event in the South China Block. *Gondwana Res.* 12 (4), 404–416. doi:10.1016/j.gr.2006.10.003

Wenzheng, J., Guimei, W., Zehong, C., Junpeng, W., Xiaoqun, Y., and Wankui, B. (2012). Key Tectonic Change Epoch and Hydrocarbon Accumulation Periods of Continental Clastic Reservoir in Sichuan Basin. *Fault-Block Oil Gas Field* 19 (3), 5.

Wu, H., Qiu, N., Chang, J., Zhang, J., and Wang, Y. (2019). Physical Simulation on Development of Multilayer Detachment Fold Belt in Eastern Sichuan, [川东多套滑脱层褶皱构造带形成物理模拟] [Article]. *Earth Sci.* 44 (3), 784–797. Article 1000-2383(2019)44:3<784:Cddtht>2.0.Tx;2-#. <Go to ISI>://CSCD:6474052. doi:10.3799/dqkx.2018.109

Xiao, A. C., Wei, G. Q., Shen, Z. Y., Wang, L., Yang, W., and Qian, J. F. (2011). Basin-mountain System and Tectonic Coupling between Yangtze Block and South Qinling Orogen [Article]. *Acta Petrol. Sin.* 27 (3), 601–611. <Go to ISI>://WOS:000289926600001.

Yan, D. P., Zhou, M. F., Song, H. L., Wang, X. W., and Malpas, J. (2003). Origin and Tectonic Significance of a Mesozoic Multi-Layer Over-thrust System within the Yangtze Block (South China) [Article]. *Tectonophysics* 361 (3-4), 239–254. doi:10.1016/s0040-1951(02)00646-7

Yin, S., Dong, L., Yang, X., and Wang, R. (2020). Experimental Investigation of the Petrophysical Properties, Minerals, Elements and Pore Structures in Tight Sandstones. *J. Nat. Gas Sci. Eng.* 76 (15), 103189. doi:10.1016/j.jngse.2020.103189

Yin, S., Lv, D. W., and Ding, W. L. (2018). New Method for Assessing Microfracture Stress Sensitivity in Tight Sandstone Reservoirs Based on Acoustic Experiments [Article]. *Int. J. Geomechanics* 18 (4), 16. Article 04018008. doi:10.1061/(asce)gm.1943-5622.0001100

Yin, S., and Wu, Z. (2020). Geomechanical Simulation of Low-Order Fracture of Tight Sandstone. *Mar. Petroleum Geol.* 117 (15), 104359. doi:10.1016/j.marpetgeo.2020.104359

Zeng, L., Gong, L., Guan, C., Zhang, B., Wang, Q., Zeng, Q., et al. (2022). Natural Fractures and Their Contribution to Tight Gas Conglomerate Reservoirs: A Case Study in the Northwestern Sichuan Basin, China. *J. Petroleum Sci. Eng.* 210 (10), 110028. doi:10.1016/j.petrol.2021.110028

Zhao, K., Jiang, P., Feng, Y., Sun, X., Cheng, L., and Zheng, J. (2021). Investigation of the Characteristics of Hydraulic Fracture Initiation by Using Maximum Tangential Stress Criterion [Investigation of the Characteristics of Hydraulic Fracture Initiation by Using Maximum Tangential Stress Criterion]. *J. Min. Strata Control Eng.* 3 (2), 14–22. doi:10.13532/j.jmsce.cn10-1638/td.20201217.001

Zheng, H., Zhang, J., and Qi, Y. (2020). Geology and Geomechanics of Hydraulic Fracturing in the Marcellus Shale Gas Play and Their Potential Applications to the Fuling Shale Gas Development. *Energy Geosci.* 1 (No.1-2), 36–46. doi:10.1016/j.engeos.2020.05.002

Conflict of Interest: LP and YZ were employed by the Sinopec Exploration Company.

The remaining authors declare that the research was conducted in the absence of any commercial or financial relationships that could be construed as a potential conflict of interest.

Publisher's Note: All claims expressed in this article are solely those of the authors and do not necessarily represent those of their affiliated organizations, or those of the publisher, the editors and the reviewers. Any product that may be evaluated in this article, or claim that may be made by its manufacturer, is not guaranteed or endorsed by the publisher.